CHEMISTRY OF MATERIALS

ARTICLE

pubs.acs.org/cm

Luminescence and Microstructural Features of Eu-Activated $LiBaPO_4$ Phosphor

Suyin Zhang,[†] Yosuke Nakai,[‡] Taiju Tsuboi,[‡] Yanlin Huang,*[,†] and Hyo Jin Seo*[,§]

[†]College of Chemistry, Chemical Engineering and Materials Science, Soochow University, Suzhou 215123, China

[‡]Faculty of Engineering, Kyoto Sangyo University, Kamigamo, Kyoto 603-8555, Japan

[§]Department of Physics, Pukyong National University, Busan 608-737, Republic of Korea

ABSTRACT: Eu^{2+}-activated $LiBaPO_4$ phosphor was synthesized by conventional solid-state reaction. The photoluminescence excitation and emission spectra, the temperature dependent luminescence intensities (12−450 K), and decay curves of the phosphor were investigated. With the increasing of temperatures, the emission bands of $LiBaPO_4$:Eu^{2+} show the abnormal blue-shift and the decreasing of emission intensity. The natures of the Eu^{2+} emission in $LiBaPO_4$, for example, the luminescence quenching temperature, and the activation energy for thermal quenching (ΔE), were reported. The afterglow fluorescence was detected in $LiBaPO_4$:Eu^{2+} phosphor. Together with the Eu^{2+} luminescence, Eu^{3+} ions with the abnormal crystal field were observed. The site-selective excitation in the $^5D_0 \rightarrow {}^7F_0$ region for Eu^{3+} ions, emission spectra, and decay curves have been investigated using a pulsed, tunable, and narrowband dye laser to detect the microstructure and crystallographic surrounding of $Eu^{3+,2+}$ at Ba^{2+} sites in $LiBaPO_4$. The multiple sites structure of Eu^{2+} and Eu^{3+} ions in $LiBaPO_4$ lattices was suggested. The lower quenching temperature, afterglow, and luminescence mechanism were discussed. The photoluminescence quantum efficiencies of $LiBaPO_4$:Eu^{2+} were measured and compared with the reported phosphors. Different from the published data on $LiBaPO_4$:Eu^{2+}, this investigation indicates that $LiBaPO_4$:Eu^{2+} is not a good phosphor candidate applied in white light emitting diode.

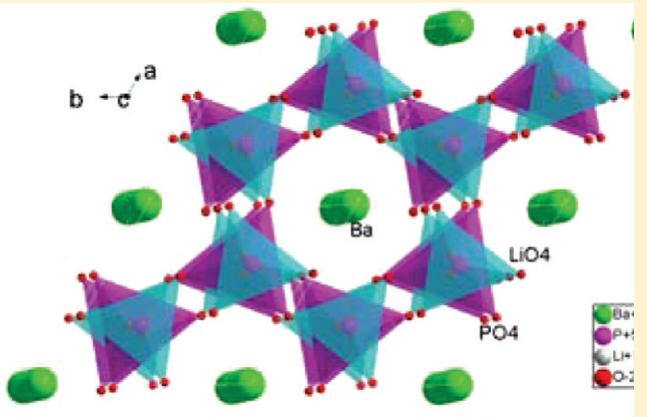

KEYWORDS: luminescence, optical materials and properties, phosphors, LED, tridymite structure

INTRODUCTION

The phosphates with $ABPO_4$ formula (A and B are mono- and divalent cations, respectively) are in a large family of monophosphates with the different structure types strictly depending on the relative size of the A and B ions.[1,2] These compounds have been considered to be efficient luminescent hosts due to their excellent thermal and hydrolytic stability.[3,4] Recently, Eu^{2+}-doped $ABPO_4$ phosphates have received much attention for the potential applications as new white light emission diodes (W-LEDs) phosphors,[4] such as $KCaPO_4$:Eu^{2+},[5] $KSrPO_4$:Eu^{2+},[6] $KBaPO_4$:Eu^{2+},[7,8] $LiSrPO_4$:Eu^{2+},[9] $NaCaPO_4$:Eu^{2+},[10] and $ABaPO_4$:Eu^{2+} (A = Na, K).[11]

$ABPO_4$ has a tridymite structure (β-SiO_2) when B is rather small and A is large,[2] for example, $LiBaPO_4$. This structure involves the existence of a 1:1 ordering between the cross-linked LiO_4 and PO_4 tetrahedra on the basis of an isotypy with the β-SiO_2 tridymite.[12] Eu^{2+}-doped compounds with tridymite structure have been confirmed to be notable for their good luminescent performance, for example, MAl_2O_4 (M = Ba, Sr, and Ca)[13,14] and $BaMgSiO_4$.[15,16] There are two barium sites Ba(1) and Ba(2) with nine-coordination in $BaAl_2O_4$ lattices. Therefore, two Eu^{2+} emission bands were observed in Eu^{2+}-doped $BaAl_2O_4$.[14,17] In the structure of $BaMgSiO_4$ there are three different Ba sites in equal amounts in the lattice. Two sites Ba(1) and Ba(2) are coordinated by nine oxygen ions, whereas the third Ba(3) is surrounded by six oxygen ions.[18] Two Eu(1) and Eu(2) in the structure of $BaMgSiO_4$ are comparable with those in $BaAl_2O_4$,[17] which give emissions at long wavelength, while the Eu(3) site shows a short emission band at 398 nm.[15] In $BaAl_2O_4$ and $BaMgSiO_4$, the Eu^{2+} luminescence is at low energies due to preferential orientation of a d orbital of Eu^{2+} ions on Ba sites in these lattices.[13] However, in $CaAl_2O_4$:Eu^{2+}, no preferential orientation of the d orbital is left due to the strongly distorted stuffed-tridymite lattice. Consequently, only a blue emission at 440 nm has been observed.[13,19] This indicates that although these compounds have the similar stuffed-tridymite-type structure, the chemically different compounds have the important influence on the Eu^{2+} luminescence.[15]

It has been confirmed that $LiBaPO_4$ is suitable for second harmonic generating (SHG) responses and shows larger SHG

Received: October 4, 2010
Published: January 19, 2011

dx.doi.org/10.1021/cm102854p | *Chem. Mater.* 2011, 23, 1216–1224

effects relative to quartz.[20] The luminescence properties of Ce^{3+}, Sn^{2+}, and Cu^{+} doped $LiBaPO_4$ have been reported.[12,21,22] Waite[23] first report the Eu^{2+} luminescence doped in $LiBaPO_4$. Just as in $BaAl_2O_4$, Eu^{2+} ions on barium sites in $LiBaPO_4$ have a preferential orientation of the d orbital. Recently, Wu et al. have reported that $LiBaPO_4$:Eu^{2+} is a good candidate phosphor applied in W-LEDs and exhibits higher thermal stability than that of commercially available $Y_3Al_5O_{12}$:Ce^{3+}.[24]

In this paper, we present an insightful investigation of the luminescence of $LiBaPO_4$:Eu^{2+}. We obtained the different results from those reported in the references.[24] In addition, the luminescence quantum efficiency, crystallographic sites, and the microstructure of Eu^{2+} ions doped in $LiBaPO_4$ are reported. The temperature dependent luminescence intensities and decay curves (12−450 K) were measured. The activation energy for thermal quenching was obtained for $LiBaPO_4$:Eu^{2+}. $LiBaPO_4$:Eu^{2+} has a lower quenching temperature, afterglow fluorescence, and changing color with increase of temperature. The characteristics indicate that this phosphor is not a candidate applied in W-LEDs. The excitation spectra have been investigated in the $^5D_0 \rightarrow {}^7F_0$ region for Eu^{3+} ions in $LiBaPO_4$ by using a pulsed, tunable, and narrowband dye laser to detect the Ba^{2+} cation sites in $LiBaPO_4$. The multiple sites structure of Eu^{2+} ions in $LiBaPO_4$ lattices was suggested and discussed.

EXPERIMENTAL SECTION

Polycrystalline samples of Eu^{2+}-doped $LiBaPO_4$ were synthesized using a conventional solid-state reaction. The starting material was a stoichiometric mixture of reagent grade $BaCO_3$, Li_2CO_3, $(NH_4)_2HPO_4$ (A.R. grade), and Eu_2O_3 (99.99% purity). First, the mixture was heated up to 350 °C in 10 h and kept at this temperature for 5 h. The obtained powder was mixed and then heated up to 750 °C for 5 h in air. After that, the sample was thoroughly mixed and heated for 10 h in a reduction atmosphere (N_2:H_2 = 95:5) at 1050 °C obtained by DTA analysis. The Eu^{2+} doped samples were prepared with the doping concentration of 5% of $BaCO_3$. The XRD pattern was collected on a Rigaku D/Max diffractometer operating at 40 kV and 30 mA with Bragg−Brentano geometry using Cu Kα radiation (λ = 1.5405 Å).

The photoluminescence excitation and emission spectra were recorded on a Perkin-Elmer LS-50B luminescence spectrometer with Monk−Gillieson type monochromators and a xenon discharge lamp used as excitation source. Luminescence spectra were recorded between 10 and 300 K on a 75 cm monochromator (Acton Research Corp. Pro-750) equipped with a helium flow cryostat and observed with a photomultiplier tube (PMT) (Hamamatsu R928). To study the thermal quenching from 20 to 500 °C, the same spectrofluorimeter was equipped with a homemade heating cell under the excitation of a 365 nm UV lamp. The luminescence decay was measured using the third harmonic (355 nm) of a pulsed Nd:YAG laser. The crystallographic site of Eu^{3+} ions in this host was investigated by the site-selective excitation measurement (for the description of the experimental method see ref 25). Quantum efficiency (QE) was measured by an Absolute Photoluminescence Quantum Yield Measurement System (C9920-02, Hamamatsu) at room temperature. The excitation was done by changing the excitation wavelength of light from a 150 W Xe lamp.

RESULTS AND DISCUSSION

Phase Formation. The X-ray diffraction (XRD) patterns of $LiBaPO_4$:Eu^{2+} together with the Joint Committee on Powder Diffraction Standards (JCPDS) card No. 14-0270 are shown in Figure 1. From a comparison between them, the position and intensity of the peaks are the same. No impurity lines were observed, and the entire pattern could be well indexed to a $LiBaPO_4$ single phase.

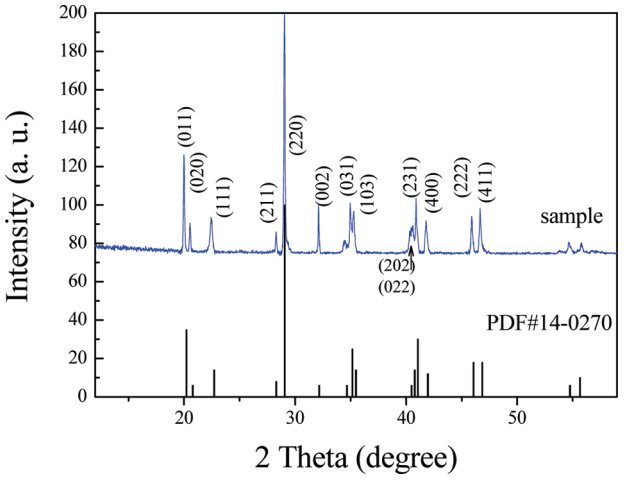

Figure 1. XRD pattern of $LiBaPO_4$:Eu^{2+} of this work and JCPDs card No.14-0270.

The material $LiBaPO_4$ belongs to the stuffed tridymite structure with a hexagonal unit cell and space group $P6_3$.[26] In this stuffed tridymite structure, each PO_4 tetrahedron is connected with four LiO_4 tetrahedrons and each LiO_4 tetrahedron is connected with four PO_4 tetrahedrons, and the two types of tetrahedrons are linked by corner sharing and build up the tridymite skeleton. As shown in Figure 2, the three-dimensional network of corner-sharing LiO_4 and PO_4 tetrahedrons forms channels in the *a*- and *c*-directions, where Ba^{2+} ions are located (Figure 2 a,b). In this structure, there are three types of Ba^{2+} sites, Ba(1), Ba(2), and Ba(3). The structure of $LiBaPO_4$ is closely related to $BaAl_2O_4$. The most important difference between them is the size of the two kinds of tetrahedra in $LiBaPO_4$ ($[LiO_4]^{7-}$ and $[PO_4]^{3-}$), whereas there is only one kind of tetrahedron in $BaAl_2O_4$ ($[AlO_4]^{5-}$).

Photoluminescence Spectra. The excitation spectra of $LiBaPO_4$:Eu^{2+} in Figure 3 by monitoring 473 and 530 nm show a broad peak from 230 to 450 nm, which can be attributed to 4f−5d transition of Eu^{2+} ions. It suggests that $LiBaPO_4$:Eu^{2+} could be effectively excited by UV chips (360−400 nm). The emission spectra of the Eu^{2+}-doped $LiBaPO_4$ under the excitation of 280 and 385 nm in Figure 3 show one emission band peaking at 485 nm, which is ascribed to the $4f^65d \rightarrow 4f^7$ ($^8S_{7/2}$) transition on Eu^{2+} ions. The phosphor presents bright green luminescence. These results agree with what was reported by Wu et al.[24,27]

The asymmetric emission spectra (λ_{ex}= 280 and 385 nm) in Figure 3 show that Eu^{2+} has more than one emission center in $LiBaPO_4$ lattices, which can be deconvoluted into at least two Gaussian components peaked at 473 and 530 nm. The emission spectrum of $LiBaPO_4$:Eu^{2+} shows no dependence of the emission spectra on the excitation wavelengths. However, the excitation spectra for the two emission bands have a noticeable difference. The rough estimation of the Stokes shifts for the emissions at 473 and 530 nm are about 5400 cm^{-1}, and 9700 cm^{-1}, respectively.

In the stuffed-tridymite-type structures, Ba ions have Ba(1) and Ba(2) in nine-coordination in $BaAl_2O_4$ or three sites Ba(1) and Ba(2) in nine-coordination and Ba(3) in six-coordination in

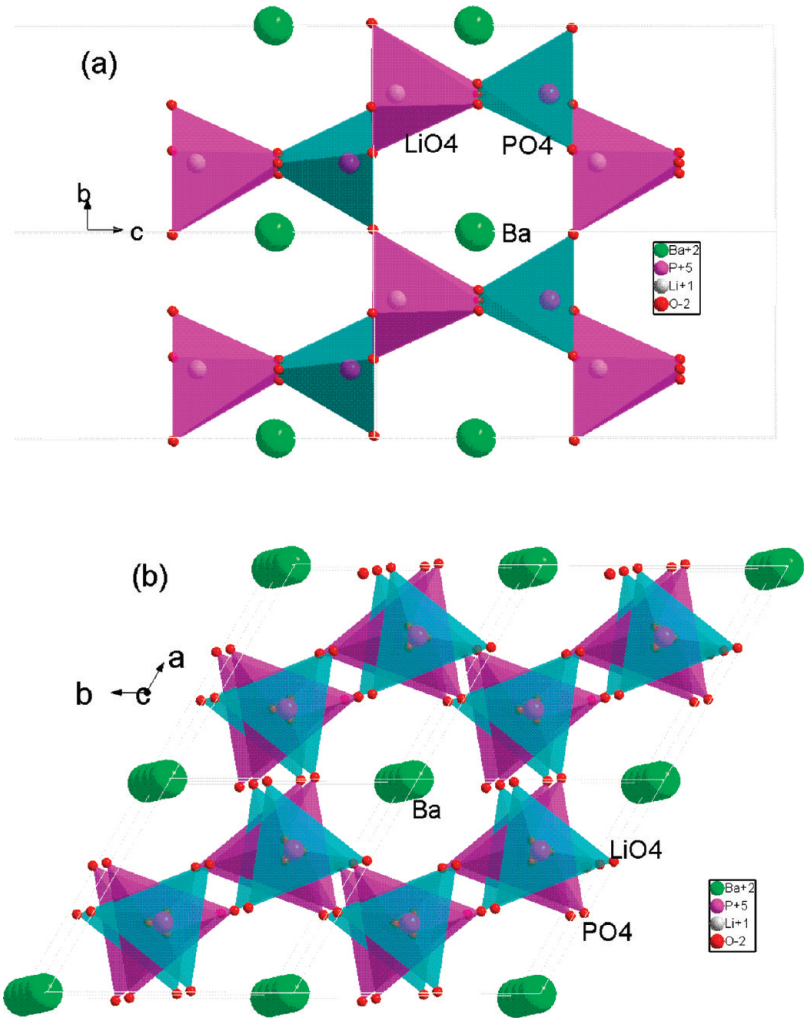

Figure 2. Schematic views of the structure of $LiBaPO_4$ along the *a*- (a) and *c*-directions (b).

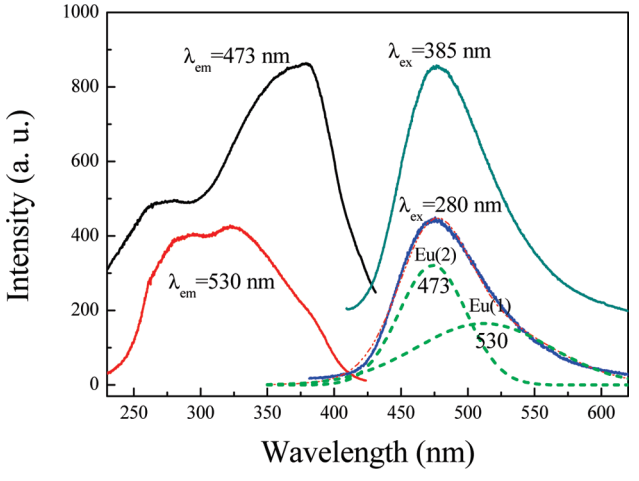

Figure 3. Excitation (λ_{em} = 473 and 530 nm) and emission spectra (λ_{ex} = 280 and 385 nm) of $LiBaPO_4:Eu^{2+}$. One emission spectrum is given by a Gaussian fit into two components.

$BaMgSiO_4$. The so-called Ba(1) and Ba(2) are distinguished by the average distance from the oxygen ions, for example, $Ba(1)-O^{2-}$ is 2.89 Å and $Ba(2)-O^{2-}$ is 2.94 Å in $BaMgSiO_4$.[18] Usually, Eu(1) and Eu(2) give emissions at long wavelength, and a short emission band is from Ba(3). For example, in $BaMgSiO_4$ there are three Eu^{2+} emissions at 502, 509, and 398 nm.[16] When the crystal environments are analogous, the Eu^{2+} center with a shorter $Eu^{2+}-O^{2-}$ distance will give a longer wavelength emission. Since the crystal environments of Eu^{2+} ions on Ba(1) and Ba(2) sites are very similar in $BaMgSiO_4$, the 502 nm emission was ascribed to the Ba(2) site, and the 509 nm to Eu^{2+} ions on the Ba(1) sites. The much higher energy of Eu^{2+} emission at 398 nm on Ba(3) sites could be explained by means of preferential orientation of a d orbital of the Eu^{2+} ion.

The luminescence spectrum at 12 K (Figure 4) consists of a broad band at 480 nm and a band at about 530 nm; in addition a small shoulder at 412 nm can be observed. At temperatures above 297 K the two longer wavelength bands are only visible, and the 412 nm emission band disappears. Analogously, it is reasonable that the Eu^{2+} emission at 473 and 530 nm could be ascribed to Ba(2)(Eu2) and Ba(1)(Eu1), respectively. And 412 nm emission is from Ba(3)(Eu3) sites, which quenches at RT similar to that in $BaMgSiO_4$. These three occupations will be confirmed by site-selective luminescence spectra of Eu^{3+} mentioned below.

Photoluminescence Quantum Efficiency (QE). The QE of a phosphor is important for its application. The QE of $LiBaPO_4$:

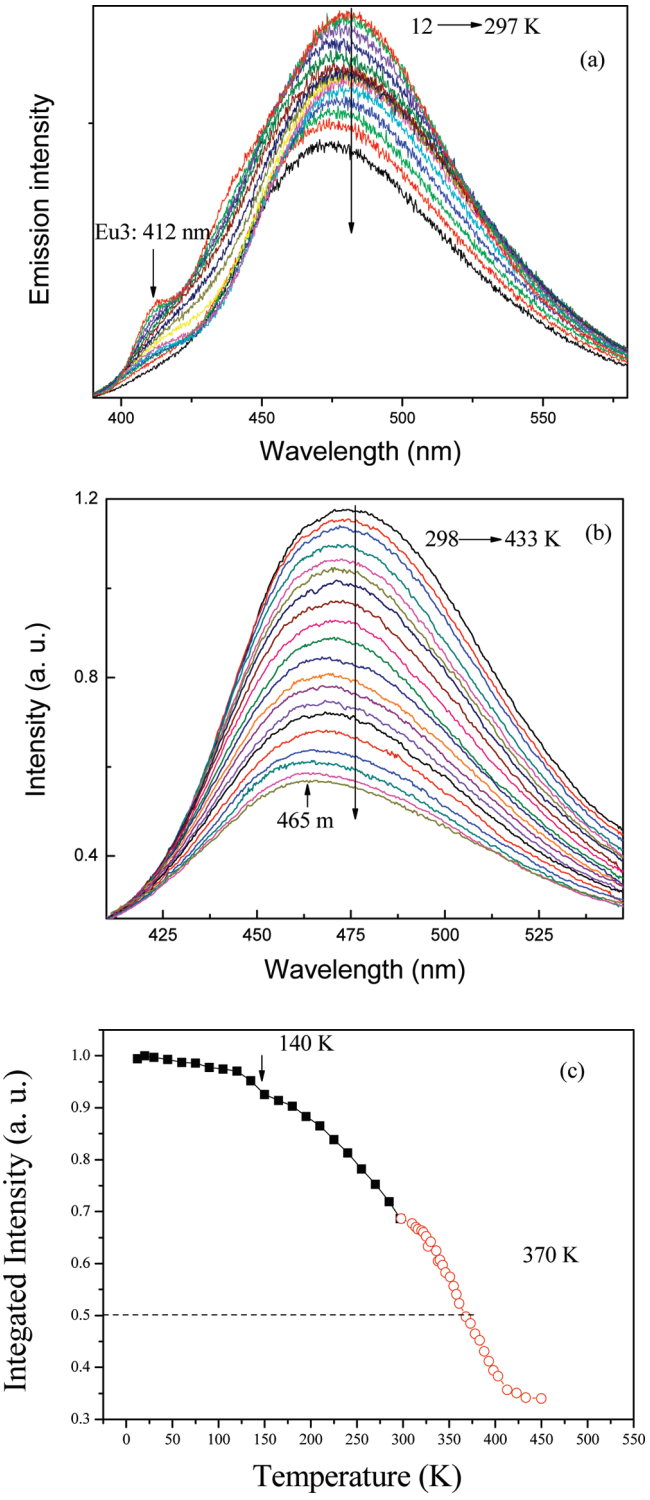

Figure 4. Emission spectra of $LiBaPO_4:Eu^{2+}$ at different temperatures (a and b) and the temperature dependence of the integrated emission intensity normalized with respect to the value at 12 K (c).

Eu^{2+} luminescence was measured to be 58.5% at the excitation of 330 nm light at 300 K. However, $LiBaPO_4:Eu^{2+}$ has a lower luminescence QE value in comparison with the reported results in some LED phosphors in Table 1. Certainly, the QE usually depends on the synthesis conditions and Eu^{2+} concentrations. The higher quantum yields can be obtained by further improving the synthesis conditions to reduce the number of defects and impurities.

Table 1. Quantum Efficiencies at Room Temperature of $LiBaPO_4:Eu^{2+}$ and the Reference Phosphors

phosphors	λ_{ex}	λ_{em}	QE (%)	
$LiBaPO_4:Eu^{2+}$	330 nm	483 nm	58.5	this work
$CaSrS:Eu^{2+}$ (1 mol %)	350 nm	663 nm	53.4	ref 28
$AlN:Eu^{2+}$ (0.10 mol %)	365 nm	465 nm	63.0	ref 29
$BaMgAl_{10}O_{17}:Eu^{2+}$ (2 mol %)	254 nm	450 nm	70.0	ref 30
$YAG:Ce^{3+}$ (mol 3%)	460 nm	560 nm	70.0	ref 31
$SrSi_2N_2O_2:Eu^{2+}$ (2 mol %)	450 nm	535 nm	91.0	ref 32

Temperature Dependent Luminescence and Thermal Quenching. In general, the temperature dependence of W-LED phosphors is important because it has great influence on the light output and color rendering index. Phosphors must sustain emission efficiency at temperatures of about 150 °C over a long term when they are used in white LEDs. It is thus required that the thermal quenching of phosphors should be small, typically for high-power ones. The thermal quenching of $LiBaPO_4:Eu^{2+}$ was evaluated by measuring the temperature-dependent emission intensities as shown in Figure 4.

The emission intensities decrease as the temperature increases as shown in Figure 4a,b. Figure 4c represents the temperature dependence of the integrated emission intensity normalized to 12 K. The thermal quenching begins during the heating at 140 K. The thermal quenching temperature, $T_{0.5}$, defined as the temperature at which the emission intensity is 50% of its original value, is 370 K. It can be seen from references that the $T_{0.5}$ for Eu^{2+}-doped $BaSi_2O_5$ is 460 K,[33] that for $Cs_2MP_2O_7$ (M = Ca, Sr) is 600 K,[33] that for $Sr_3(PO_4)_2$ and $Ba_3(PO_4)_2$ is >550 K,[34] that for $SrSi_2O_2N_2$ is 600 K,[35] and that for $KBPO_4:Eu^{2+}$ (B = Sr, Ba) is 673 K.[4] The $T_{0.5}$ for iso-structural $BaMgSiO_4:Eu^{2+}$ is 300 K.[15] In comparison with the reported phosphors, $LiBaPO_4:Eu^{2+}$ has a relatively lower quenching temperature.

P. Dorenbos has proposed that the main mechanism responsible for the thermal quenching of Eu^{2+} luminescence in solids is the ionization of the electron from the lowest energy level of the relaxed Eu^{2+} $4f^65d^1$ electronic configuration to the host lattice conduction band level.[36] Following this suggestion, it is responsible that the thermally activated ionization from the $4f^65d$ state is for temperature quenching of the luminescence in $LiBaPO_4:Eu^{2+}$. The temperature dependence of the luminescence intensity is described by a modified Arrhenius equation as following equation:[37]

$$I_T = \frac{I_0}{1 + c\exp\left(-\frac{\Delta E}{kT}\right)} \quad (1)$$

where I_0 is the initial emission intensity, I_T is the intensity at different temperatures, ΔE is activation energy of thermal quenching, c is a constant for a certain host, and k is the Boltzmann constant (8.629×10^{-5} eV). The activation energy is the energy required to raise the electron from the relaxed excited level into the host lattice conduction band. Figure 5 plots $\ln[(I_0/I_T) - 1]$ versus $1000/T$ for $LiBa_{0.95}Eu_{0.05}PO_4$. According to eq 1, the activation energy ΔE was calculated to be 0.03 eV. Moreover, in Figure 4a,b the wavelength of the maximum emission shifts toward blue region from 480 to 465 nm with increasing temperature. This

dx.doi.org/10.1021/cm102854p |Chem. Mater. 2011, 23, 1216–1224

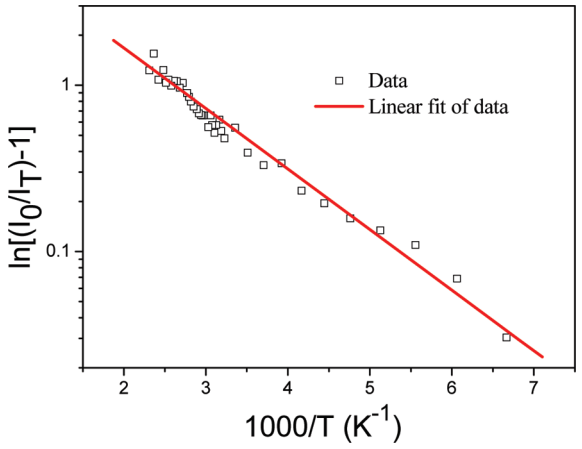

Figure 5. Activation energy of the thermal quenching of $LiBaPO_4:Eu^{2+}$ phosphor fitted in eq 1.

shift with increasing temperature is indicative of the chromatic instability of $LiBaPO_4:Eu^{2+}$.

Temperature Dependent Luminescence Lifetimes. Figure 6a shows the luminescence decay curves of $LiBaPO_4:Eu^{2+}$ at different temperatures. The decays display nearly exponential curves. The luminescence lifetimes of the Eu^{2+} ions are calculated as a function of temperature and displayed in Figure 6b. On the base of the suggested mechanism for the thermal quenching of Eu^{2+} is the ionization of the electron from the lowest energy level of the relaxed Eu^{2+} $4f^65d^1$ electronic configuration to the host lattice conduction band level.[36] The activation energy (ΔE) for thermal quenching of the Eu^{2+} was also determined by measuring the temperature dependence of the Eu^{2+} emission lifetime. The drawn line in the figure is fitted to the equation as[33]

$$\tau(T) = \frac{\tau_r}{1 + [\tau_r/\tau_{nr}] \exp(-\Delta E/kT)} \quad (2)$$

where k is the Boltzmann constant and τ_r and τ_{nr} are radiative and nonradiative decay times. The thermal activation energy for thermal quenching (ΔE) is fitted to be 0.032 eV. This is matched with the calculation in eq 1.

In Figure 6b, the luminescence lifetime of Eu^{2+} is near a constant (around 820 ns) from 12 K up to 240 K and then drops at higher temperature, presenting a typical temperature quenching behavior. The rapid shortening of the Eu^{2+} emission lifetime for $T > 240$ K indicates the onset of nonradiative transitions, which may be a thermal ionization and/or energy transfer process. In the case of thermal ionization, the electron in the excited 5d state of the Eu^{2+} auto-ionizes into the conduction band and is delocalized. This is responsible for the observed quenching. The calculated activation energy of 0.03 eV indicates that the thermal energy required to promote an electron from the lowest excited state of Eu^{2+} to the host lattice conduction band is not high.[36]

As shown above, $LiBaPO_4:Eu^{2+}$ does not show the stable luminescence at high temperature. This is not in agreement with the reported results by Wu et al.:[24,27] $LiBaPO_4:Eu^{2+}$ with the $T_{0.5}$ of 450 K has higher thermal stability than commercially available $YAG:Ce^{3+}$. However, our results are similar to that recently reported for $LiSrPO_4:Eu^{2+}$ phosphor by Lin et al.:[4] $LiSrPO_4:Eu^{2+}$ has worse thermal stability than $KBaPO_4:Eu^{2+}$ and $KSrPO_4:Eu^{2+}$. This was explained that Li^+ promotes the

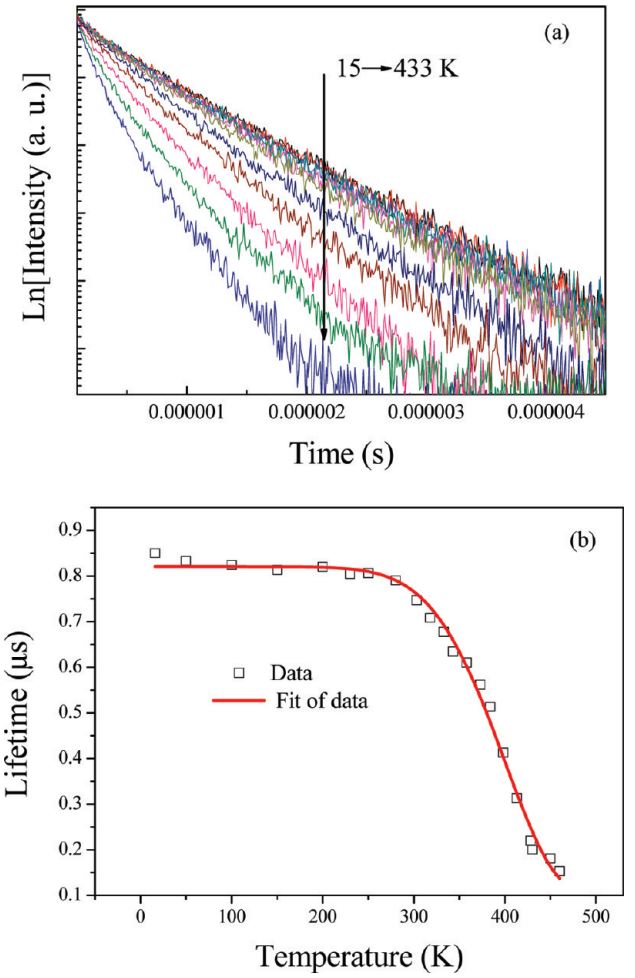

Figure 6. Luminescence decay curves of $LiBaPO_4:Eu^{2+}$ phosphor under the excitation of 355 nm of a pulsed Nd:YAG laser at 15 to 433 K (a) and the temperature dependent lifetimes of the Eu^{2+} emission fitted into eq 2 (b).

conversion of Eu^{2+} to Eu^{3+} more than K^+ ion does, based on electronic affinity.

A low $T_{0.5}$ and low activation energy of $LiBaPO_4:Eu^{2+}$ might be related to the lowest energy level of the Eu^{2+} $4f^65d^1$ electronic configuration not being well isolated from the host lattice conduction band. Recently, Lin et al.[4] have elucidated the luminescent intensity of activators in $ABPO_4$ phosphors at various temperatures with reference to crystal structure and the coordination environment. In this case, the microstructure and crystallographic surrounding of Eu^{2+} ions at Ba^{2+} sites should be understood.

Afterglow and Emission Spectra from Eu^{3+}. The afterglow in $LiBaPO_4:Eu^{2+}$ can be obviously seen after switching off the excitation of a UV lamp. The afterglow decay curve (Figure 7) is detected after the irradiation of UV light (254 nm). The curve can be fitted into a biexperimental decay function, indicating at least two decay processes: a fast decay (15 s) and a slow decay (79 s). It is probably due to the existence of traps with appropriate depth, and the related work is being carried on. These results suggest that electrons and holes produced by UV excitation move back to Eu^{2+} sites in the crystals through thermal hopping and tunneling and recombine radiatively at Eu^{2+} sites. Such afterglow was also reported in Eu^{2+}-doped Ba_2SiO_4 and Ba_3SiO_5 crystals.[38]

dx.doi.org/10.1021/cm102854p |*Chem. Mater.* 2011, 23, 1216–1224

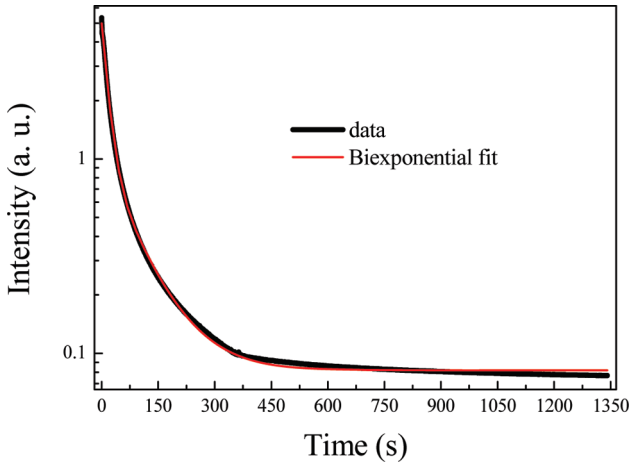

Figure 7. Experimental afterglow curve of $LiBaPO_4:Eu^{2+}$ phosphor.

Actually, in $LiBaPO_4:Eu^{2+}$, besides the Eu^{2+} ions, the emission from Eu^{3+} also existed. From the time-resolved spectra, the Eu^{3+} luminescence can be distinctly displayed as shown in Figure 8a. Under the time delay of 50 μs, the emission transitions $^5D_0-^7F_{0,1,2}$ from Eu^{3+} ions can be observed. And the stronger Eu^{3+} emission can be observed with the decrease of Eu^{2+} emission by monitoring after a long delay time after laser excitation. This indicates that actually two different valence states, +2, and +3, are available for Eu in $LiBaPO_4:Eu^{2+}$. Figure 8b shows the very different lifetimes for the Eu^{2+} and Eu^{3+} ions; therefore, the time-resolved spectra can separate their emission.

It should also be remarked that although the $LiBaPO_4:Eu^{2+}$ sample was obtained in a reduction atmosphere, this reduction could not be completely realized. Under reducing conditions, Eu^{2+} ions can be stable on alkaline earth metal sites. However, when Eu^{2+} ions are heated within a certain temperature range, they may be oxidized as $Eu^{2+} \rightarrow Eu^{3+} + e^-$. Therefore, a luminescence of the Eu^{3+} can exist. The phenomenon is related to the crystal structure and the coordination environment of the activators at different temperatures.

In oxide matrixes the $(4f)^n \rightarrow (4f)^{n-1}(5d)^1$ transitions usually occur in the UV spectral region for Ln^{3+} ions and in the visible region for Ln^{2+} ions. They are parity allowed, and therefore their intensity is many times higher than that of the 4f−4f transitions that may be masked completely. Therefore, the PL spectra do not show any signature of Eu^{3+} in the sample under the excitation of continued wavelength, which means the Eu^{3+} luminescence is suppressed. Tang and Chen[11] recently reported this phenomenon in Eu^{2+} doped $ABaPO_4:Eu$ ($A = Na^+, K^+$). XPS results show that Eu^{2+} and Eu^{3+} ions coexist in these compounds even though the spectra of Eu^{3+} were not observed in that work.

The emission spectra of Eu^{3+} doped in $LiBaPO_4$ shown in Figure 8a present the abnormal features: the unusual high energy position (573 nm, 17 452 cm^{-1}) and the abnormal relative intensity (many times stronger than the $^5D_0 \rightarrow {}^7F_1$) for the forbidden $^5D_0 \rightarrow {}^7F_0$ transition. Usually, this observation is connected with the charge-compensating oxide ion and experience of an abnormal crystal field (CF) around the Eu^{3+} ions.[39] In such a situation an unusual crystal field is expected, affecting both the energy-level location and the relative intensity of the radiative transitions from the $^5D_0$ level.

Site-Selective Spectra and Discussions. $BaLiPO_4$ belongs to the stuffed tridymite structures which are derived from the

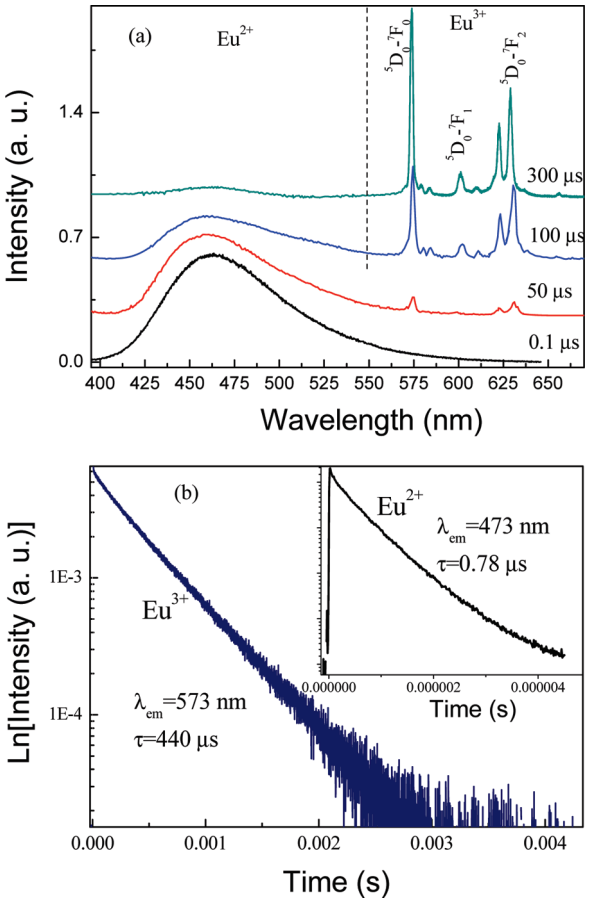

Figure 8. Time-resolved spectra $LiBaPO_4:Eu^{2+}$ measured at different delay times after the laser excitation as labeled in part (a) and the luminescence decay curves from Eu^{2+} and Eu^{3+} in $LiBaPO_4:Eu^{2+}$ (b).

structure of β-SiO_2. The structure consists of tetrahedral SiO_4 units which are linked together through corner sharing of all four oxygen atoms of each tetrahedron, thereby creating a one-dimensional six-ring channel. P^{5+} and Li^+ replace Si^{4+} in the tetrahedra of the SiO_2 tridymite; Ba^{2+} will occupy sites in channels parallel to the *c*-axis.[23] In the tetrahedra network, each PO_4 shares four corners with LiO_4 tetrahedra. Thus, the tetrahedra form a six-membered ring, and Ba cations occupy the channels running through the tetrahedral network. Although the crystal structure of $BaLiPO_4$ is similar to trydimite, the direction of tetrahedra is different.

It is interesting to further investigate whether or not the abnormal crystal field (CF) around the Eu^{3+} ions can be kept in $LiBaPO_4$ prepared in air atmosphere. Eu^{3+} ($4f^6$ configuration) is largely used as a probe of the surrounding symmetry because the emission and excitation lines between $^5D_0$ and $^7F_0$ levels are nondegenerate.[40] By site-selective excitation and emission spectra, the presence of crystallographic nonequivalent sites in a given host matrix can be revealed, for example, three Eu^{2+} sites in $LiBaPO_4$ lattices. This is helpful to elucidate the luminescence mechanism of the Eu^{2+} ion by revealing the microstructure and crystallographic surrounding.

The Eu sites in $LiBaPO_4$ were revealed by the excitation spectra of the $^7F_0 \rightarrow {}^5D_0$ transition of Eu^{3+} ions in $LiBaPO_4$ obtained by heating the same sample of $LiBaPO_4:Eu^{2+}$ in air atmosphere. Figure 9 shows the excitation spectra corresponding

dx.doi.org/10.1021/cm102854p |*Chem. Mater.* 2011, 23, 1216–1224

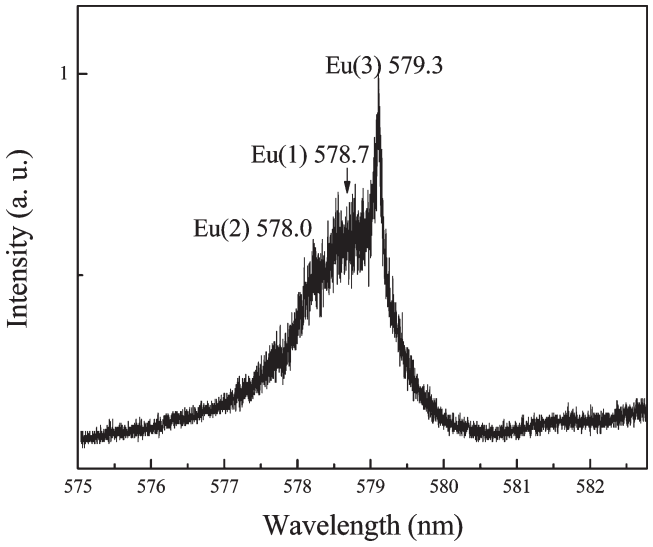

Figure 9. Excitation spectra for $^7F_0 \rightarrow {}^5D_0$ transition of Eu^{3+} in $LiBaPO_4$:Eu^{3+} by monitoring the total luminescence.

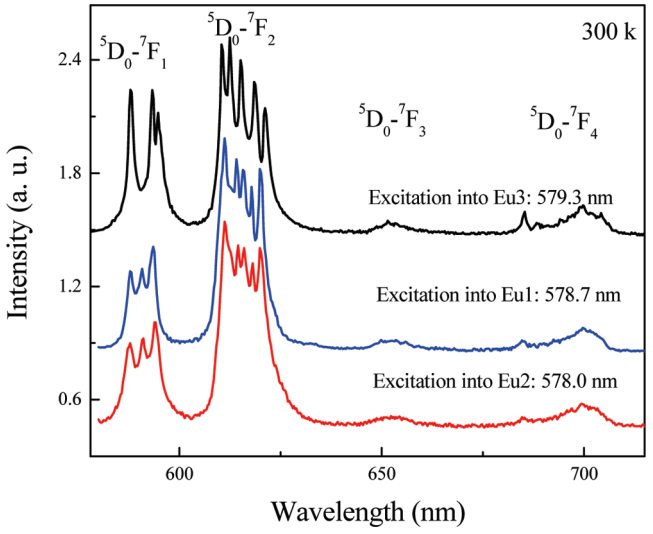

Figure 10. Site-selective emission spectra of $^5D_0 \rightarrow {}^7F_J$ (J = 1, 2, 3, 4) for $LiBaPO_4$:Eu^{3+} by exciting into site Eu(1): 578.0 nm, Eu(2): 578.7 nm, and Eu(3): 579.3 nm.

to the $^7F_0 \rightarrow {}^5D_0$ transition, obtained by monitoring the total luminescence of Eu^{3+} ions. The $^7F_0 \rightarrow {}^5D_0$ excitation spectra consist of the transition lines at 578.0, 578.7, and 579.3 nm. Usually in an ionic system, the position of the $^5D_0 \rightarrow {}^7F_0$ transition level of Eu^{3+} depends on the ionicity of the system and the size and coordination of the Eu^{3+} or Sm^{2+} site. The high coordination and the long metal−oxygen atomic distance for Eu^{3+} in the lattice are responsible for the high energy of the $^5D_0$ level.[41]

In the stuffed-tridymite-type structures, the crystal environments of Eu^{2+} ions on Ba1 and Ba2 sites are similar and the Ba(2)−O^{2-} distance is longer than that of Ba(1)−O^{2-}.[18] Therefore, the $^7F_0 \rightarrow {}^5D_0$ transitions at 578.0 and 578.7 are ascribed to Ba(2)(Eu2) and Ba(1)(Eu1), respectively. And Ba(3)(Eu3) sites are attributed to the 579.3 nm transition line. The results in Figure 9 clearly indicate that the Eu^{3+} ions occupy three intrinsic

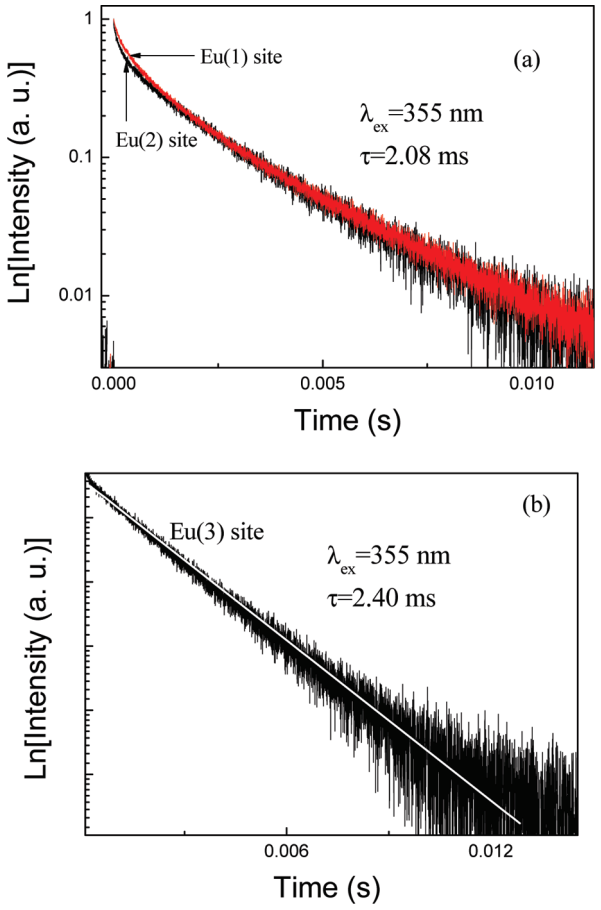

Figure 11. $^5D_0 \rightarrow {}^7F_2$ luminescence decay curves under the excitation of sites Eu(2): 578.0 nm and Eu(1): 578.7 nm (a) and Eu(3): 579.3 nm (b).

crystallographic sites in $LiBaPO_4$. Although the microstructure around the Eu^{2+} and Eu^{3+} ions doped in $LiBaPO_4$ could be different because of the different charge compensations in the same host, however, the conclusion of the at least three Eu^{2+} sites occupying on Ba^{2+} in $LiBaPO_4$ could be reasonable.

The site-selective emission spectra were recorded by tuning the laser to resonance with each excitation peak of the sites Eu(2) (578.0 nm), Eu(1) (578.7 nm), and Eu(3) (579.3 nm) (in Figure 10). The two spectra for site-selective excitation into sites Eu(2) and Eu(1) have nearly the same profile with the same emission wavelength position. The strongest emission line is the $^5D_0 \rightarrow {}^7F_2$ transition at 614 nm for two sites. However, the spectrum for Eu3 has a different profile. Actually, this characteristic can also be supported by the fluorescence decay curves for each site. Figure 11 shows decay curves of $^5D_0 \rightarrow {}^7F_2$ emission under excitation in sites Eu(2) (578.0 nm), Eu(1) (578.7 nm), and Eu(3) (580.3 nm). The decay curves for sites Eu(2) and Eu(1) exhibit the nearly same lifetime of 2.08 ms with a small difference in the initial part. The luminescence curve for Eu(3) has a good exponential decay with a longer lifetime of 2.4 ms.

It can be suggested that the Eu(1) and Eu(2) positions of the Eu^{3+} ions in $LiBaPO_4$ were arranged in the similar environment. This property can be explained by the high disordering of the cation positions on Eu(1) and Eu(2). This can be seen from the excitation spectra in Figure 9 and emission spectra in Figure 10; the broadening of the fluorescence lines observed can be

explained in terms of the channel in this structure which is occupied by Eu ions resulting in a larger local distortion and greater disorder over the whole structure. It seems that the Eu atoms occupy a family of sites with identical oxygen environments.

In $LiBaPO_4$, two Eu^{2+} sites can be detected at room temperature; however, three Eu^{3+} emissions can be observed in $LiBaPO_4$:Eu^{3+}. This indicates that the Eu^{3+} ions in $LiBaPO_4$ are more stable than the Eu^{2+} ions in the same host. The instability luminescence of Eu^{2+} ions can be also reflected by the recent reports in rare earth ion doped $ABPO_4$ phosphors.[4] It has been reported that the $LiSrPO_4$:Eu^{2+} phosphor has worse thermal stability than $KSrPO_4$:Eu^{2+} and $KBaPO_4$:Eu^{2+}. This was explained as because Li^+ promotes the conversion of Eu^{2+} to Eu^{3+} more than the K^+ ion. It can be suggested that in Eu^{2+} doped $LiBaPO_4$, Li^+ promotes the conversion of Eu^{2+} to Eu^{3+} and the activation energy of the conversion of Eu^{2+} to Eu^{3+} is not high.

Lin et al.[4] also reported that the $LiSrPO_4$:Tb^{3+} phosphors have higher luminescence stabilities than those of $KSrPO_4$:Tb^{3+} and $KBaPO_4$:Tb^{3+}. They explain that trivalent Tb^{3+} in $ABPO_4$ forms a competitive hole-trapping center as has been confirmed by the detection of lattice defect levels. When the trivalent cation (Tb^{3+} or Eu^{3+}) was doped in the divalent cation (B site) in $ABPO_4$, an electron is required to the charge compensation. Then $LiSrPO_4$:Tb^{3+} must have the best thermal stability because the Li^+ ion captures more electrons than the K^+ ion or Na^+. This can explain the reason why the emissions for three Eu^{3+} sites in $LiBaPO_4$ are all stable at RT. As Lin et al.[4] suggested, the thermal stabilities of all of $ABPO_4$ compounds could be determined from the crystal structure and the coordination environment of the rare-earth metal. Although the real quenching mechanism for Eu^{2+} doped $LiBaPO_4$ phosphor is not yet understood in detail, the knowledge of the site distribution over the different sites of the structure in this work would be useful to deeply analyze the luminescence quenching mechanisms in $ABPO_4$. To further the study, some new investigations are needed, for example, band structures and density of states (DOS) of pure $LiBaPO_4$, orbital distributions of atoms, the detailed coordination environment of Eu, charge transfer band, and exchange interaction acting on the Eu.

CONCLUSIONS

In conclusion, the green phosphor Eu^{2+}-doped $LiBaPO_4$ was synthesized by the high temperature solid state method. The photoluminescence excitation and emission spectra, the temperature dependent luminescence intensities (12−450 K), and the decay curves of the phosphor were measured. The excitation of $LiBaPO_4$:Eu^{2+} with a broad band from 230 to 450 nm, could be effectively excited by UV chips (360−400 nm). The luminescence spectra show that Eu^{2+} ions have three emission centers in the $LiBaPO_4$ lattices, which are Eu(1) at 530 nm, Eu(2) at 473 nm, and Eu(3) at 415 nm. The quantum efficiency of $LiBaPO_4$:Eu^{2+} was 58.5% at the excitation of 330 nm. The luminescence of $LiBaPO_4$:Eu^{2+} shows a typical thermal quenching effect with a $T_{0.5}$ value of 370 K. From the dependences of luminescence intensities and lifetimes on temperature, the thermal activation energy of $LiBaPO_4$:Eu^{2+} was calculated to be 0.03 eV. Some emission features of $LiBaPO_4$:Eu^{2+}, that is, the afterglow, the Stokes shift, and the color shift for thermal quench ing were discussed. Three cation sites for the Eu^{2+} and Eu^{3+} emission in $LiBaPO_4$ host lattices were suggested. This structural feature was confirmed by the emission spectra and the excitation spectra of the $^7F_0 \rightarrow {}^5D_0$ transition of probe Eu^{3+} ions in $LiBaPO_4$. The microstructure of Eu doped in $LiBaPO_4$ was discussed on the basis of the crystal structure and the luminescence spectra. This could be helpful for understanding the mechanisms responsible for the quenching of luminescence at high temperature and for developing new materials that have potential application for white LEDs.

AUTHOR INFORMATION

Corresponding Author

*E-mail: hjseo@pknu.ac.kr (H.J.S.), huang@suda.edu.cn (Y.H.).

ACKNOWLEDGMENT

This work was supported by Program for Postgraduates Research Innovation in University of Jiangsu Province (2010), China, and by Midcareer Researcher Program through National Research Foundation (NRF) grant funded by the Ministry of Education, Science and Technology (MEST) (No. 2009-0078682).

REFERENCES

(1) Ben Amara, M.; Vlasse, M.; Le Flem, G.; Hagenmuller, P. *Acta Crystallogr., Sect. C* **1983**, *39*, 1483.
(2) Elammari, L.; El Koumiri, M.; Zschokke-Gränacher, I.; Elouadi, B. *Ferroelectrics* **1994**, *158*, 19.
(3) Chan, T. S.; Liu, R. S.; Baginskiy, I. *Chem. Mater.* **2008**, *20*, 1215.
(4) Lin, C. C.; Xiao, Z. R.; Guo, G. Y.; Chan, T. S.; Liu, R. S. *J. Am. Chem. Soc.* **2010**, *132*, 3020.
(5) Zhang, S. Y.; Huang, Y. L.; Seo, H. J. *J. Electrochem. Soc.* **2010**, *157*, 261.
(6) Tang, Y. S.; Hu, S. F.; Lin, C. C.; Bagkar, N. C.; Liu, R. S. *Appl. Phys. Lett.* **2007**, *90*, 151108.
(7) Im, W. B.; Yoo, H. S.; Vaidyanathan, S.; Kwon, K. H.; Park, H. J.; Kim, Y. I.; Jeon, D. Y. *Mater. Chem. Phys.* **2009**, *115*, 161.
(8) Lin, C. C.; Tang, Y. S.; Hu, S. F.; Liu, R. S. *J. Lumin.* **2009**, *129*, 1682.
(9) Wu, Z. C.; Shi, J. X.; Gong, M. L.; Wang, J.; Su, Q. *Mater. Chem. Phys.* **2007**, *103*, 415.
(10) Qin, C. X.; Huang, Y. L.; Shi, L.; Chen, G. Q.; Qiao, X. B.; Seo, H. J. *J. Phys. D: Appl. Phys.* **2009**, *42*, 185105.
(11) Tang, W. J.; Chen, D. H. *J. Am. Ceram. Soc.* **2009**, *92*, 1059.
(12) Boutinaud, P.; Parent, C.; Le Flem, G.; Moine, B.; Pedrini, C. *J. Mater. Chem.* **1996**, *6*, 381.
(13) Poort, S. H. M.; Blokpoel, W. P.; Blasse, G. *Chem. Mater.* **1995**, *7*, 1547.
(14) Hörkner, V. W.; Müller-Buschbaum, H.; Allg, Z. A. *Chem.* **1979**, *451*, 40.
(15) Poort, S. H. M.; Reijnhoudt, H. M.; Kuip, H. O. T.; Blasse, G. *J. Alloys Compd.* **1996**, *241*, 75.
(16) Peng, M. Y.; Pei, Z. W.; Hong, G. Y.; Su, Q. *J. Mater. Chem.* **2003**, *13*, 1202.
(17) Huang, S.; Von Der Mühll, R.; Ravez, J.; Chaminade, J.; Hagenmuller, P.; Couzi, M. *J. Solid State Chem.* **1994**, *109*, 97.
(18) Liu, B.; Barbier, J. *J. Solid State Chem.* **1993**, *102*, 115.
(19) Dougill, M. W. *Nature* **1957**, *180*, 292.
(20) Liang, C. S.; Eckert, H.; Gier, T. E.; Stucky, G. D. *Chem. Mater.* **1993**, *5*, 597.
(21) Boutinaud, P.; Duloisy, E.; Pedrini, C.; Moine, B.; Parent, C.; Le Flem, G. *J. Solid Slate Chem.* **1991**, *94*, 236.
(22) Wanmaker, W. L.; Spier, H. L. *J. Electrochem. Soc.* **1962**, *109*, 109.
(23) Waite, M. S. *J. Electrochem. Soc.* **1974**, *121*, 1122.
(24) Wu, Z. C.; Liu, J.; Gong, M. L.; Su, Q. *J. Electrochem. Soc.* **2009**, *156*, 153.
(25) Ding, H. Y.; Huang, Y. L.; Shi, L.; Seo, H. J. *J. Electrochem. Soc.* **2010**, *157*, 54.

(26) Elamman, L.; Elouadi, B.; Muller-Vogt, G. *Phase Transitions.* **1988**, *13*, 29.
(27) Wu, Z. C.; Liu, J.; Guo, Q. J.; Gong, M. L. *Chem. Lett.* **2008**, *37*, 190.
(28) Xia, Q.; Batentschuk, M.; Osvet, A.; Winnacker, A.; Schneider, J. *Radiat. Meas.* **2010**, *45*, 350.
(29) Inoue, K.; Hirosaki, N.; Xie, R. J.; Takeda, T. *J. Phys. Chem. C.* **2009**, *113*, 9392.
(30) Stevels, A. L. N. *J. Lumin.* **1978**, *17*, 121.
(31) Bachmann, V.; Ronda, C.; Meijerink, A. *Chem. Mater.* **2009**, *21*, 2077.
(32) Bachmann, V.; Ronda, C.; Oeckler, O.; Schnick, W.; Meijerink, A. *Chem. Mater.* **2009**, *21*, 316.
(33) Srivastava, A. M.; Comanzo, H. A.; Camardello, S.; Chaney, S. B.; Aycibin, M.; Happek, U. *J. Lumin.* **2009**, *129*, 919.
(34) Poort, S. H. M.; Meijerink, A.; Blasse, G. *J. Phys. Chem. Solids* **1997**, *58*, 1451.
(35) Bachmann, V.; Jüstel, T.; Meijerink, A.; Ronda, C.; Schmidt, P. J. *J. Lumin.* **2006**, *121*, 441.
(36) Dorenbos, P. *J. Phys.: Condens. Matter.* **2005**, *17*, 8103.
(37) Baginskiy, I.; Liu, R. S. *J. Electrochem. Soc.* **2009**, *156*, 29.
(38) Yamaga, M.; Masui, Y.; Sakuta, S.; Kodama, N.; Kaminaga, K. *Phys. Rev. B.* **2005**, *71*, 205102.
(39) Vikhnin, V. S.; Liu, G. K.; Beitz, J. V. *Phys. Lett. A* **2001**, *287*, 419.
(40) Macfarlane, R. M. Shelby, R. M. In *Spectroscopy of Solids Containing Rare Earth Ions*; Kaplyanskii, A. A., Macfarlane, R. M., Eds.; North-Holland: Amsterdam, 1987; p 51.
(41) Meijerink, A.; Dirksen, G. J. *J. Lumin.* **1995**, *63*, 189.